Collision-Energy-Resolved Penning Ionization Electron Spectroscopy of Phenylacetylene and Diphenylacetylene by Collision with He*(2^3S) Metastable Atoms

Andriy Borodin, Masakazu Yamazaki, Naoki Kishimoto, and Koichi Ohno*

Department of Chemistry, Graduate School of Science, Tohoku University, Aramaki, Aoba-ku, Sendai 980-8578, Japan

Received: June 26, 2005; In Final Form: September 7, 2005

Penning ionization of phenylacetylene and diphenylacetylene upon collision with metastable He*(2^3S) atoms was studied by collision-energy-/electron-energy-resolved two-dimensional Penning ionization electron spectroscopy (2D-PIES). On the basis of the collision energy dependence of partial ionization cross-sections (CEDPICS) obtained from 2D-PIES as well as ab initio molecular orbital calculations for the approach of a metastable atom to the target molecule, anisotropy of interaction between the target molecule and He*(2^3S) was investigated. For the calculations of interaction potential, a Li(2^2S) atom was used in place of He*(2^3S) metastable atom because of its well-known interaction behavior with various targets. The results indicate that attractive potentials localize in the π regions of the phenyl groups as well as in the π-conjugated regions of the acetylene group. Although similar attractive interactions were also found by the observation of CEDPICS for ionization of all π MOs localized at the C≡C bond, the in-plane regions have repulsive potentials. Rotation of the phenyl groups about the C≡C bond can be observed for diphenylacetylene because of a low torsion barrier. So the examination of measured PIES was performed taking into consideration the change of ionization energies for conjugated molecular orbitals.

I. Introduction

Understanding the dynamics of chemical processes and reactions is of fundamental importance. In the particular case of chemi-ionization processes known as the Penning ionization,[1−3] the ionization of a target atom or molecule (M) occurs by collision with a metastable atom (A*). Important information on the dynamics of this process can be obtained by the energy analysis of ejected electrons

$$A^* + M \rightarrow A + M_i^+ + e^- \qquad (1)$$

The number of positive ions generated in the experiment determines the total ionization cross-sections for the target molecules, which were already studied well in previous works.[4−11] The observed bands can be assigned to particular ionic states by using the electron spectroscopic technique; in eq 1, an *i*th state is symbolized by M_i^+. The relative ratio of the partial ionization cross sections can be observed by an electron spectroscopic technique that is known as the Penning ionization electron spectroscopy (PIES).[12] Usually, ionic states can be related to valence molecular orbitals (MOs). In the Penning ionization process, an electron in MO having higher electron density outside the boundary surface of M is transferred to the inner-shell orbital of A*, which, according to the electron exchange model,[13] results in a high-intensity band in PIES.[14]

The relative band intensity in PIES is determined by the probability of the Penning ionization process, which, in turn, is thought to be proportional to the overlapping between the unoccupied 1s MO of He*(2^3S) and a self-consistent field MO localized outside the collision boundary surface. Thus, the relative ratio of ionization cross-sections can be estimated by the calculation of orbital reactivity with exterior electron density[14,15] $(EED)_i$ for *i*th MO (φ_i)

$$(EED)_i = \int_\Omega |\varphi_i(r)|^2 \, dr \qquad (2)$$

where Ω is the space outside the repulsive molecular surface.

The combination of the electron energy analysis with the velocity selection of A*[16−19] has made it possible to observe the collision energy dependence of partial ionization cross-sections (CEDPICS) as well as the collision-energy-resolved PIES (CERPIES). Since the time-of-flight (TOF) method has an advantage in simultaneous measurement of CEDPICS and CERPIES in the collision-energy-/electron-energy-resolved two-dimensional PIES (2D-PIES),[20] the TOF method was adapted in our group rather than the velocity-controlled-supersonic-jet-beam method.[21−23]

The obtained CEDPICSs can be connected to the anisotropic interaction between a target molecule M and a metastable atom A*. In the case of positive CEDPICS, the metastable atom with larger kinetic energy reaches the inner region of the target against a repulsive interaction. Thus, the MO region corresponding to the positive CEDPICS can be connected to a repulsive interaction. On the other hand, negative CEDPICS can be assigned to an attractive interaction around the corresponding MO region, since the metastable atom is deflected to the target molecule by the attractive interaction. In this case, the number of deflected trajectories decreases with the increase of collision energy. For the target molecule, since the electron distributions of individual MOs are more or less localized on the special parts of the molecule, different CEDPICSs for various ionic states can be connected to the anisotropy of interaction between the molecule and the metastable atom.

On the other hand, the peak energy shift in PIES or CERPIES with respect to the ionization band in the ultraviolet photoelectron spectroscopy (UPS) can also provide information on the

* To whom correspondence should be addressed. Tel.: +81-22-795-6578. Fax: +81-22-795-6580. E-mail address: ohnok@qpcrkk.chem.tohoku.ac.jp.

10.1021/jp053469v CCC: $33.50
Published on Web 01/19/2006

anisotropy of interaction. According to the model of two potential curves for the Penning ionization processes,[2] for interdistance R at which the excitation transfer occurs, electron energy E_e is equal to the energy difference between the incoming potential curve $V^*(R)$ for the entrance channel ($A^* + M$) and the outgoing potential curve $V^+(R)$ for the exit channel ($A + M^+$), provided that the relative translational energy is conserved during the transfer of electron excitation. The position of the peaks measured in PIES can be therefore analyzed as follows

$$E_e(R) = V^*(R) - V_i^+(R) = E_A^* - [IP_i(\infty) + \Delta IP_i(R)] \quad (3)$$

where E_A^* is the excitation energy of an atomic probe, A* (19.82 eV for $He^*(2^3S)$), and $IP_i(\infty)$ is the ionization potential for the ith ionic state of an isolated molecule and is most commonly determined by means of UPS. At last, $\Delta IP_i(R)$ accounts for the shift in the IP due to interactions between the molecular target and the probe

$$\Delta IP_i = V^*(\infty) - V_i^+(\infty) - [V^*(R) - V_i^+(R)] \quad (4)$$

In the case of $A^* = He^*(2^3S)$, the anisotropic interaction potential curves V^* for the approach of $He^*(2^3S)$ to the molecular target along various directions can also be obtained by model potential calculations with a $Li(2^2S)$ atom, based on the well-known resemblance[24−26] between $He^*(2^3S)$ and $Li(2^2S)$ species in collision processes.

Moreover, the ab initio molecular orbital calculations with $Li(2^2S)$[27,28] may also be applied to the simulation of the 2D-PIES data, including CERPIES and CEDPICS. For those simulations the entrance and exit potential energy surfaces, ionization widths, classical trajectories (taking into consideration the rotation motions and a so-called impact parameter b), etc. should be calculated. A good agreement between the experimental and calculated data even for relatively large molecules such as CH_3CN[27] and C_6H_6[28] allows us to use the calculated interaction potential curves V^* for the analysis of the CEDPICS directly.

In this way, to obtain information on the anisotropic interaction of $He^*(2^3S)$ with various molecules and chemical functional groups, a number of compounds has been investigated in our group in recent years.[29−34] The obtained results allow us to reveal some tendencies in anisotropic interaction with $He^*(2^3S)$: the attractive interaction around the lone pair electrons[30−32] close to π regions for unsaturated hydrocarbons[30] and for heterocyclic compounds,[33] the repulsive interaction around C−H bonds of alkyl groups.[34]

In this study, we have investigated 2D-PIES of phenylacetylene ($C_6H_5C{\equiv}CH$) and diphenylacetylene (tolane, $C_6H_5C{\equiv}CC_6H_5$). These compounds have been studied in photochemistry in relation to π-electron conjugation. Since the two phenyl groups of diphenylacetylene are flexible at room temperature, the torsional motion of the C ≡ C bond of this compound has been studied by the laser spectroscopy in a supersonic cooled jet.[35] The potential barrier height for torsional rotation was also reported to be 202 cm^{-1}.

In the case of the ground-state cation of diphenylacetylene ($^2B_{3u}$), the barrier height for the torsional motion becomes much larger (1980 ± 60 cm^{-1}).[36] For the C≡C stretching modes[37] of diphenylacetylene, Raman spectroscopic techniques have been utilized in the lowest excited triplet state (1974 cm^{-1}) with the nanosecond time-resolved spontaneous Raman spectroscopy[38] and in the excited singlet states (1557, 1577, and 2099 cm^{-1}) with the coherent anti-Stokes Raman scattering.[39] For the investigations of ionic states of these molecules, the HeI ultraviolet photoelectron spectroscopy (UPS) was used.[40−42] In these studies, UPS spectra of phenylethylenes and related compounds were investigated. The correlation between the highest four π bands was examined for various phenylacetylenes, and vibrational structures in some bands were connected[41] to the stretching of the C≡C bond. It was also noticed[42] for diphenylacetylene that some π bands should broaden when changing the ionization energies with rotation of the two phenyl groups around the C≡C bond at room temperature. The features of UPS were discussed[42] in terms of eigenvalues of the ionization energies calculated by a semiempirical method (SPINDO) for various dihedral angles between the two phenyl groups of diphenylacetylene. In PIES, the reactivity of valence MOs can be examined with the EED model calculations depending on the dihedral angles around the C≡C bond of diphenylacetylene. It would be interesting to obtain information on the electronic structure of π conjugated compounds as well as anisotropic interaction around the phenyl groups and the C≡C triple bond compared with related compounds such as benzene, acetylene, biphenyl, etc.[28,43−46]

II. Experimental Section

The experimental apparatus used for measurements is described in detail in previous papers.[16−19,29] Briefly, metastable $He^*(2^3S)$ atoms were produced by a discharge nozzle source. In addition, a water-cooled helium discharge lamp was used for quenching the metastable $He^*(2^1S)$ atoms generated as a byproduct in the source. To obtain the collision-energy-resolved spectra, a pseudorandom chopper disk[47] rotating with a frequency of about 400 Hz modulated the beam of the metastable helium atoms. For the UPS measurements, the apparatus was equipped with an additional source of photons from the HeI resonance line (584 Å, 21.22 eV).

The interaction between the vapor of the molecules under investigation and the metastable $He^*(2^3S)$ atoms as well as with the HeI photons occurred in a small collision cell (20 mm in diameter). A hemispherical electrostatic deflection type analyzer connected to the collision cell was used to measure the kinetic energy of the ejected electrons. The energy resolution was determined by the measurement of the full width at half-maximum (fwhm) of the Ar^+ ($^2P_{3/2}$) peak. The value of fwhm was about 60 meV for the UPS and PIES measurements in the higher-resolution mode and about 200 meV for the 2D-PIES measurement in the lower-resolution mode. The transmission curve for the energy analyzer was calibrated on the basis of the relative peak intensities for various compounds with respect to known UPS data.[48,49] The spectra were measured for the gas phase of compounds evaporated at room temperature. Because of the low saturated vapor pressure of diphenylacetylene (it is solid at room temperature), the collecting time for the spectra was rather long.

The collision energy dependence of the partial ionization cross-section was obtained for a specific ionic state in 2D-PIES accumulated as a function of two parameters, electron kinetic energy (E_e) and collision energy (E_c) between A* and M. The cuts of the 2D spectrum at selected ionization bands give CEDPICSs, while the cuts of the 2D spectrum at selected collision energies provide CERPIESs. In the 2D-PIES measurement, TOF spectrum I_e at a given scanning electron kinetic energy was accumulated. For the determination of the $He^*(2^3S)$ velocity v_m, another measurement for intensity I_m of the secondary electrons from a stainless steel plate inserted into the collision cell was employed. The relative partial ionization cross-section $\sigma(E_e,v_r)$ can be determined by the equations

$$\sigma(E_e,\nu_r) = c(I_e(E_e,\nu_m)/I_m(\nu_m))\,(\nu_m/\nu_r) \quad (5)$$

$$\nu_r = (\nu_m{}^2 + 3k_bT/m)^{1/2} \quad (6)$$

where c is a constant, ν_r is the relative velocity of collision adjusted for the average velocity of the target molecules with mass m at temperature T, and k_b is the Boltzmann constant. Finally, $\sigma(\nu_r)$ is converted to $\sigma(E_c)$ by the relationship

$$E_c = \mu\nu_r{}^2/2 \quad (7)$$

where μ is the reduced mass of the system.

III. Calculations

The IP values of an isolated target molecule were calculated with high accuracy by the outer valence Green's functions (OVGF) method[50−52] with 6-311++G** and 6-311+G* basis sets for phenylacetylene and diphenylacetylene, respectively. The molecular geometry for these calculations was selected from the experimental data[53,54] based on the microwave spectroscopy and electron diffraction for phenylacetylene and diphenylacetylene, respectively.

Moreover, a simulation of PIES was performed by the exterior electron density values (EED)[15] for the band intensity of diphenylacetylene with the 6-31++G basis set and phenylacetylene with the 6-311++G** basis set combined with IPs by the OVGF calculation for diphenylacetylene and by UPS for phenylacetylene. The bandwidth was assumed to be 410 meV (fwhm), and the Gaussian-type functions were adapted in the simulation of PIES.

To calculate interactions between a metastable He*(2^3S) atom and a target, Li(2^2S) was used (based on the resemblance with He*(2^3S)[24−26]). The interaction potential between a molecule and the approaching Li(2^2S) was also obtained by the ab initio MO calculations. The calculations of interaction potential $V(R)$, where R is the distance from the Li atom to the investigated part of the molecule, were carried out using the second-order Møller−Plesset perturbation theory (MP2) with the standard basis sets: 6-311++G** for phenylacetylene and 6-31G** for diphenylacetylene. Moreover, to correct the basis set superposition errors (BSSE), the full counterpoise (CP)[55] method was applied.

All presented ab initio calculations were performed by the Gaussian 03 quantum chemistry package.[56]

IV. Results

In Table 1, the following data are listed for the investigated compounds: the IP values, the EED values, the slope parameters m of CEDPICS obtained in the collision energy range 90−270 meV, and the PIES peak energy shifts[57] ΔE, which may be directly connected to ΔIP_i according to eq 4. The values of ΔE were determined as the difference between the measured electron energies and the ones calculated on the basis of IP from the UPS data with respect to the excitation energy difference between PIES and UPS (21.22−19.82 = 1.4 eV). In Table 2, the OVGF IP values and the EED values are listed for five dihedral angles φ from 0 to 90° with a step of 22.5°.

The EED simulation spectrum for a diphenylacetylene molecule (one part of it may rotate relative to the other) was synthesized by summing the EED spectra for the molecule fixed at various φ (the first column of Table 2) with respect to weighting factors shown in the last column of Table 2. The weighting factors were roughly calculated as follows: For every torsional level,[35] the range of dihedral angles φ was calculated. For the angular ranges obtained as well as for free rotation, the probability of observing $P_{obs}(\varphi)$ for the molecule in states with a certain dihedral angle φ was estimated; it was performed for the room temperature (experimental conditions) on the basis of potential V for torsional rotation[35]

$$V = {}^1/_2V_B\,(1 - \cos 2\varphi) \quad (8)$$

with $V_B = 202$ cm^{-1}. The probabilities for free rotation and for oscillation at each level were calculated by the Boltzmann factor. A double integral for the product of these probabilities and $P_{obs}(\varphi)$ over all possible motions and over the region around selected dihedral angle φ in the range $\varphi \pm 11.25°$ gave the probability $P_{\varphi\pm11.25°}$ for observing the molecule in states with φ from this range as listed in Table 2. Since the spectra for molecules with dihedral angles $+\varphi$ and $-\varphi$ were identical, the factors of the EED spectra (calculated for φ = 0, 22.5, 45, 67.5, and 90°) were equal to $P_{\varphi\pm11.25°}$ for φ = 0 and 90° and to double $P_{\varphi\pm11.25°}$ for φ = 22.5, 45, and 67.5°. Table 2 presents the values of weighting factors for each dihedral angle.

TABLE 1: Assignment of Bands, IPs Calculated by OVGF (Pole Strength in Parentheses) and Observed by UPS, Peak Energy Shift ΔE for Observed Bands in PIES and UPS with Respect to the Difference between Excitation Energies (19.82 eV and 21.22 eV), and Slope Parameter m for Phenylacetylene and Diphenylacetylene

phenylacetylene							diphenylacetylene					
band	orbital character	IP UPS/eV	IP OVGF/eV (p.s.)	EED/%	ΔE/eV	m	band	orbital character	IP UPS/eV	IP OVGF/eV (p.s.)	ΔE/eV	m
1	$3b_1(\pi)$	8.84	8.74 (0.90)	5.32	−0.12	−0.12	1[a]	$4a(\pi)$	8.09	7.68−8.28	−0.16	−0.11
2	$1a_2(\pi)$	9.51	9.30 (0.89)	6.00	−0.06	−0.13	2[a]	$3a(\pi)$	9.23	9.05	−0.11	−0.21
							3[a], 4[a]	3b, 4b (π)	9.23	8.3−9.3	−0.11	−0.21
3	$8b_2(\pi)$	10.34	10.24 (0.89)	5.33	−0.09	−0.12	5[a]	$2b(\pi)$		9.56−10.48		−0.23
4	$2b_1(\pi)$	11.03	10.93 (0.88)	5.53	−0.14	−0.20	6[a]	$2a(\pi)$	10.28	10.82−10.48	−0.15	−0.22
5	$7b_2(\sigma)$	(12.00)	12.40 (0.90)	1.82	(0.01)	0.10	7, 8	$20a_g$, $19a_g$	11.67	12.10 (0.89), 12.09 (0.89)	(0.03)	0.09
6	$15a_1(\sigma)$	(12.00)	12.48 (0.89)	1.55	(0.01)	0.10	9, 10	$19b_u$, $18b_u$	11.84	12.25 (0.90), 12.35 (0.80)	(0.03)	0.09
7	$1b_1(\pi)$	12.61	12.84 (0.81)	5.10	−0.14	−0.21	11[a], 12[a]	1a, 1b(π)	12.45	12.20−12.75	−0.06	−0.19
							S_1	($\pi\pi^*$)				−0.21
8	$6b_2$	14.33	14.60 (0.88)	2.52	0.08		13, 14	$18a_g$, $17b_u$	14.08	14.36 (0.87), 14.38 (0.87)	(0.03)	
9	$14a_1$	14.62	14.84 (0.88)	1.92	(0.06)		15, 16	$17a_g$, $16b_u$		14.48 (0.87), 14.84 (0.87)		
10	$5b_2$	15.08	15.23 (0.87)	0.65	−0.11		17, 18	$16a_g$, $15b_u$	14.87	14.88 (0.86), 15.04 (0.86)	(−0.08)	
11	$13a_1$	15.75	16.20 (0.86)	1.66	0.00		19, 20	$15a_g$, $14b_u$	15.51	15.97 (0.86), 16.26 (0.85)	−0.05	
							S_2					−0.10
12	$12a_1$	16.67	17.29 (0.86)	2.12	−0.01		21	$14a_g$	16.82	17.35 (0.85)	−0.02	
13	$11a_1$	17.55	18.18 (0.89)	1.74	−0.04							

[a] IP values by the OVGF method are shown in Table 2.

TABLE 2: OVGF IP (Pole Strength in Parentheses), EED Values for π MOs of Diphenylacetylene, and Weighting Factors for Simulating the Total EED Spectrum Together with (in Parentheses) the Probabilities $P_{\varphi\pm11.25°}$ in Finding the States in the Range of the Dihedral Angle $\varphi \pm 11.25°$ for the Planes of the Phenyl Rings for Diphenylacetylene

	1		2		3		4		5		6		11		12		
bands	4a		3a		4b		3b		2b		2a		1b		1a		
φ/ degree	IP OVGF/eV (p.s.)	EED/ %	IP OVGF/eV (p.s.)	EED/ %	IP OVGF/eV (p.s.)	EED/ %	IP OVGF/eV (p.s.)	EED/ %	IP OVGF/eV (p.s.)	EED/ %	IP OVGF/eV (p.s.)	EED/ %	IP OVGF/eV (p.s.)	EED/ %	IP OVGF/eV (p.s.)	EED/ %	weighting factors ($P_{\varphi\pm11.25°}$)
0	7.68	4.67	9.04	5.87	9.05	5.90	9.31	5.10	9.56	4.23	10.82	5.00	12.20	4.98	12.75	4.84	0.22
	(0.885)		(0.881)		(0.881)		(0.880)		(0.882)		(0.854)		(0.884)		(0.807)		(0.34)
±22.5	7.77	4.62	9.05	5.90	9.05	5.92	9.10	4.92	9.75	4.43	10.80	4.99	12.35	4.85	12.74	4.84	0.35
	(0.885)		(0.881)		(0.881)		(0.882)		(0.880)		(0.855)		(0.828)		(0.807)		(0.28)
±45	7.84	4.62	9.05	5.92	8.80	5.13	8.86	5.55	10.03	4.62	10.74	4.97	12.42	4.71	12.70	4.80	0.24
	(0.885)		(0.882)		(0.883)		(0.883)		(0.876)		(0.858)		(0.819)		(0.809)		(0.19)
±67.5	8.03	4.62	9.06	5.90	8.42	4.69	9.05	5.91	10.28	4.74	10.63	4.92	12.49	4.68	12.64	4.76	0.15
	(0.885)		(0.883)		(0.885)		(0.883)		(0.871)		(0.862)		(0.816)		(0.811)		(0.12)
90	8.28	4.64	9.05	5.90	8.28	4.64	9.06	5.92	10.48	4.84	10.48	4.84	12.57	4.70	12.57	4.71	0.04
	(0.885)		(0.885)		(0.884)		(0.884)		(0.867)		(0.867)		(0.813)		(0.813)		(0.07)

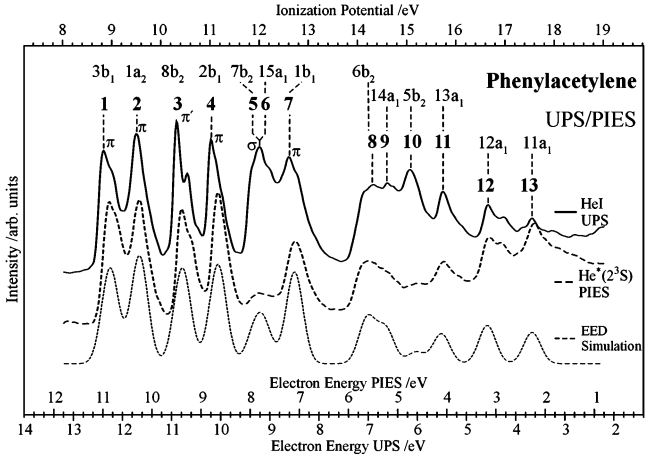

Figure 1. HeI UPS and He*(2^3S) PIES and EED simulation for the PIES of phenylacetylene.

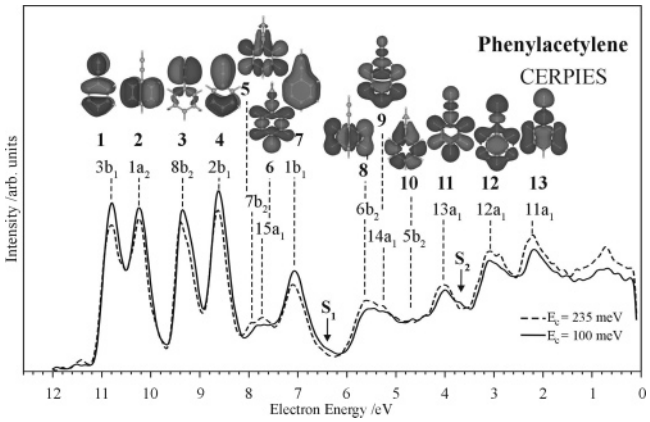

Figure 2. CERPIES of phenylacetylene (solid curve at $E_c \approx 100$ meV and dashed at $E_c \approx 235$ meV), electron density maps for MOs.

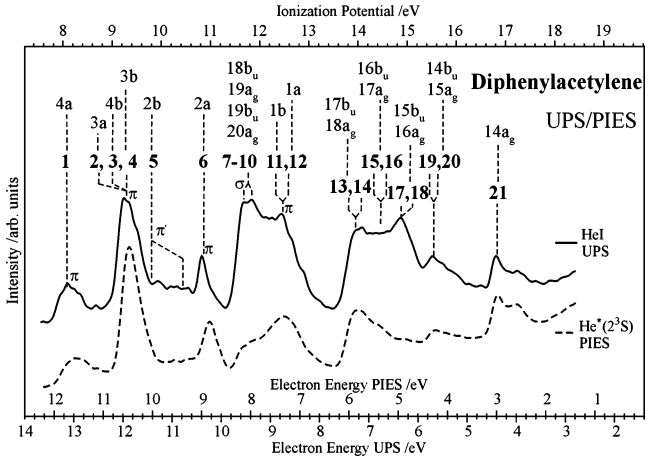

Figure 3. HeI UPS and He*(2^3S) PIES spectra of diphenylacetylene.

Figure 1 shows the UPS, the PIES, and the EED simulation for PIES of phenylacetylene. The scales of electron kinetic energy (E_e) for PIES and for UPS are shifted against each other by the difference of the excitation energies, 21.22 − 19.82 eV = 1.40 eV. Figure 3 shows the UPS and the PIES of diphenylacetylene. The EED simulation for the PIES of diphenylacetylene and the corresponding MOs are shown in Figure 5. The rotation of the phenyl groups in diphenylacetylene causes a change of conjugated π MOs. The electron density maps for the six highest MOs as well as the IPs calculated for some dihedral angles by the OVGF method are represented in Figure

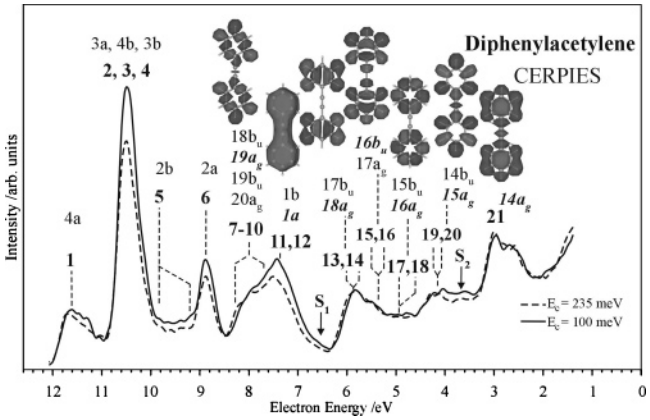

Figure 4. CERPIES of diphenylacetylene (solid curve at $E_c \approx 100$ meV and dashed at $E_c \approx 235$ meV). Electron density maps corresponding to the bands are in bold italic font.

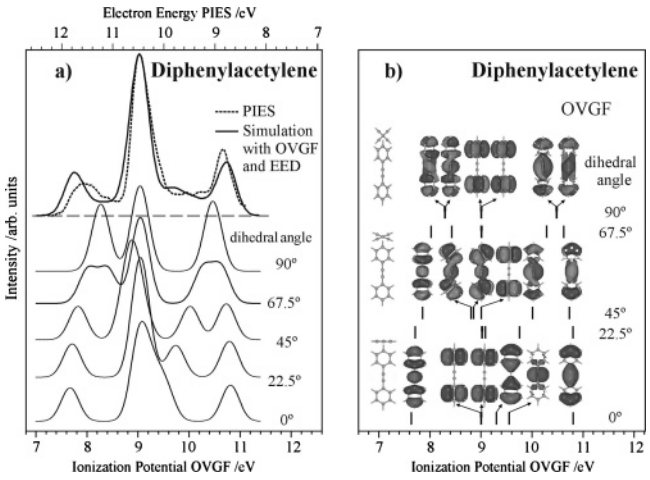

Figure 5. (a) He*(2^3S) PIES spectrum (broken line) for the electron kinetic energy region of 8.5−14 eV compared with OVGF-based EED-simulated spectra (solid line). EED spectra for various dihedral angles φ between the two phenyl groups ($\varphi = 0$, 22.5, 45, 67.5, and 90°) are also shown. (b) Calculated IPs (bars) by OVGF for various dihedral angle φ ($\varphi = 0$, 22.5, 45, 67.5, and 90°) and electron density maps for MOs 1−6 for dihedral angles $\varphi = 0$, 45, and 90°.

5b. Figure 5a presents the PIES and EED spectra for $\varphi = 0$, 22.5, 45, 67.5, and 90° combined with the OVGF ionization energies. The EED spectra are shown with reference to the low axis of IP. For the PIES spectrum, the upper axis of the electron kinetic energy is used. Both axes are shifted against each other by −0.27 eV, so the visual positions for the highest peaks in EED and in PIES are identical. For the simulation of the summarized EED spectrum, the weighting factors from Table 2 were adapted.

Figures 2 and 4 represent the spectra of CERPIES as well as the electron density maps for MOs connected to observed bands. The solid lines show the PIES spectra for the lower-collision energy range from 80 to 120 meV (an average of 100 meV), while the dashed lines show the PIES spectra for the higher-collision energy range (from 200 to 270 meV with an average of 235 meV). The calculated electron density maps are shown above the corresponding peaks for phenylacetylene. According to the OVGF calculations, the positions and the shapes for bands 7−21 of diphenylacetylene do not change significantly during internal rotation around the C≡C bond, so the most stable planar configuration has been chosen for the presentation of these MOs. Moreover, most of the selected MOs are split in two having similar electron density distributions but the opposite sign of

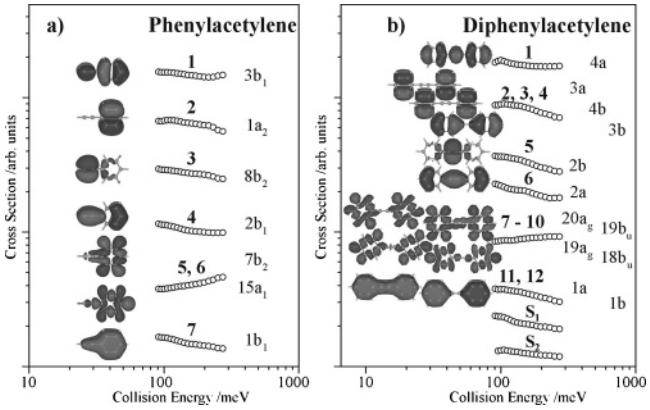

Figure 6. Collision energy dependence of the partial ionization cross sections for (a) phenylacetylene and (b) diphenylacetylene by collision with He*(2^3S).

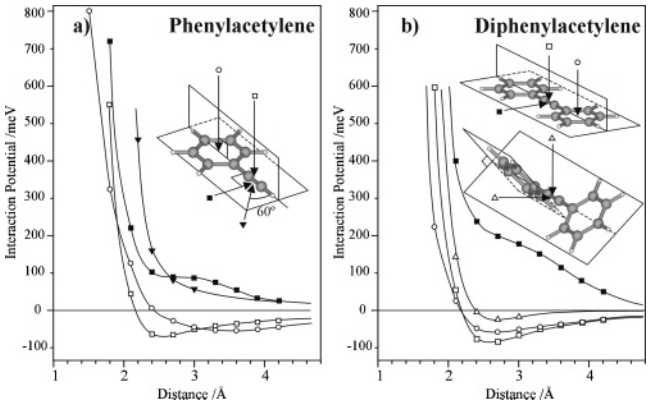

Figure 7. Interaction potential curves for (a) phenylacetylene and (b) diphenylacetylene calculated for Li(2^2S) approaching centers of the benzene ring and C≡C bonds. Distances are measured from these points to the Li atom.

the wave functions for one phenyl group. Thus, for bands 7−21, only one of each couple is presented in Figure 4; those MOs are in bold print.

On the basis of the change of the peak height for higher collision energy spectra relative to those for lower collision energy, a negative change was observed for the π bands and the slope of the negative dependence as reflected in CEDPICS (Figure 6). The CEDPICS data were obtained from the two-dimensional spectra within an appropriate range of E_e (typically the fwhm of the respective band) to avoid the effect of neighboring bands. For the bands that may not be separated (5 and 6 for phenylacetylene, 2−4, 7−10, and 11−12 for diphenylacetylene), a total CEDPICS is shown. The electron density maps are presented for all analyzed MOs next to the curves; for diphenylacetylene, the planar configuration is chosen again.

For the MP2 Li model potential calculations, out-of-plane directions approaching the phenyl and acetylene groups as well as in-plane directions approaching the acetylene group were selected. Moreover, approaches from orthogonal directions to the C≡C bond for the orthogonal configuration of diphenylacetylene ($\varphi = 90°$) was also calculated. The obtained interaction potential curves are presented in Figure 7 for the approach to the center of a ring or the C≡C bond.

V. Discussion

Phenylacetylene. The OVGF calculation results in 13 ionic states for the valence ionization of phenylacetylene in the available excitation energy range. As shown in Figure 1, most

of them, except for bands 5 and 6 ($\Delta IP = 0.05$ eV), can be distinctly detected in UPS. The positions of peaks calculated by the OVGF method agree well with the positions observed by UPS; the differences between the calculated and observed IPs are smaller than 0.27 eV for bands 1−10, which allows us to assign the observed ionic states reasonably by using the OVGF method. One might have some difficulties assigning ionic states to bands 5−7, because the observed peak position of band 7 is very close to those calculated for bands 5−7. In any case, the EED simulation spectra can help us to confirm the assumed assignment.

An EED spectrum synthesized by using this assignment and the peak position from PIES is also shown in Figure 1. Regardless of the fact that EED is a simple model that does not consider, for example, the phase of MOs or the vibrational structure, a good agreement between EED and PIES can be easily noticed. The EED intensity for bands 5 and 6 should be reduced because of the spatial alternations for the sign of the wave function, the nodal planes, whose activity against He*-(2^3S) is low. Moreover, it is noticeable that the band vibrational structure can be resolved not only for the highest four bands[38−40] but also for other well-resolved bands except for band 2 $1a_2$; their fwhm value was used for the simulation of all EED spectra in this work.

Compared to UPS, PIES has strong enhancement of the relative band intensities for MOs having the π character. An additional feature of these bands can be well illustrated by CERPIES. It is easy to notice the decrease in ionization intensity from the lower collision energy to the higher collision energy range, which indicates an attractive interaction between the metastable He* atom and the π regions of phenylacetylene. Other MOs have slightly positive collision energy dependences of the cross sections. Thus, for qualitative analysis by CEDPICS, the first seven most important MOs were selected.

Structurally, a phenylacetylene molecule contains two parts: a phenyl group and an acetylene group. Interactions with He*-(2^3S) for both parts have already been investigated separately.[28,43−45] The main attention in this paper is paid to these components. Their contribution to the total interaction with He*(2^3S)/Li(2^2S) can be illustrated by the model potential calculation (Figure 7a). It is evident from Figures 2, 6a, and 7a that an attractive interaction can be localized around the π regions of the phenyl group. The Li model potential calculation shows a well depth of 57 meV for the approach to the middle point of benzene ring. It is interesting that analogous approach to the middle point of benzene shows a more attractive character[28] with a well depth of 107 meV. The next attractive region may be localized around the C≡C bond. The calculations were performed for out-of-plane and for in-plane approach of Li(2^2S). The in-plane directions show a repulsive character, while the out-of-plane direction is attractive with a well depth of 65 meV. An acetylene molecule has, of course, an axial symmetry and equivalent character for approach to the middle of the C≡C bond from both directions (they are orthogonal to each other and to the C≡C bond); the interaction is attractive with a well depth of ∼60 meV.[43,44] Therefore, it can be concluded that π conjugation between the phenyl and acetylene groups breaks the spatial isotropy of the interaction around the C≡C bond.

A detailed study of the interaction between phenylacetylene and He*(2^3S) can be done by analysis of CEDPICS. The slope in double logarithmic coordinates for the CEDPICS of an MO can be connected with the character of interaction between the metastable He* and the region of the target related to this MO. Indeed, in the case of attractive interaction with an atomic target, the long-range attractive part of the interaction curve V^* at interdistance R can be approximated by the following relationship

$$V^*(R) \approx R^{-s} \tag{9}$$

The collision energy dependence of ionization cross sections can be represented[2−3,6] by

$$\sigma(E_c) \approx {E_c}^{-2/s} \tag{10}$$

or in the following form

$$\log \sigma(E_c) \approx -2/s \log E_c \tag{11}$$

Figure 6a presents CEDPICS for bands 1−7, while slope values (m) for the log(σ) vs log(E_c) plots are listed in Table 1.

Two MOs of phenylacetylene are localized on the specific parts of the molecule: they are π band 2 ($1a_2$) of the phenyl group and band 3 ($8b_2$), which belongs to the acetylene group. Although the MO connected to band 3 is localized in the molecular plane, it has a typically π character behavior; therefore, it was marked as π'. These MOs also have similar slopes of CEDPICS ($m = -0.13$ and $m = -0.12$). It looks natural that band 1 ($3b_1$) also has a similar value of the CEDPICS slope ($m = -0.12$). This π MO distributes in both groups; the parts of this MO localize on the phenyl and acetylene groups and are divided by a nodal plane; in fact, this MO is a spatial sum of two independent parts. An opposite case is presented in the MOs corresponding to bands 4 ($2b_1$) and 7 ($1b_1$). In these MOs, the sign of the wave function is the same for both C atoms that connect the phenyl and acetylene groups. So the resulting MOs are spread over the whole molecule and their CEDPICS slopes reach $m = -0.20$ and $m = -0.21$ for bands 4 ($2b_1$) and 7 ($1b_1$), respectively. Therefore, π conjugation between the phenyl and acetylene groups reinforces the effective attractive interaction potential in the π regions of the target.

Diphenylacetylene. In fact, a diphenylacetylene molecule has one more phenyl group than phenylacetylene. Geometrically, the planar structure with D_{2h} symmetry is optimal, but a small barrier for rotations about the C≡C bond allows us to observe this molecule in states with various dihedral angles φ between the planes of the phenyl groups ($\varphi = 0-90°$). The ab initio calculation at MP2 level using the 6-31G* basis set results in a value for barrier height (V_B) of 0.023 eV (184 cm^{-1}); the result of experimental estimation[35] is $V_B = 202$ cm^{-1}.

Rotation should have an essential influence on π conjugated MOs; while σ MOs, according to the OVGF calculations, show only weak IP dependences (less than 0.01 eV) on dihedral angle φ. Such a weak degree of conjugation allows us to assume that σ MOs should have ionization energies and shapes of peaks similar to those of phenylacetylene. The PIES and UPS spectra of diphenylacetylene presented in Figure 3 confirm it. Most of the bands, except for bands 1, 4−6, and 21, are split in two; those are different in the sign of the wave function for one of the phenyl groups. So it is not difficult to assign bands 1 and 6−21 by OVGF analogously with phenylacetylene, of course, taking into consideration all the merged bands. For a detailed assignment and understanding of the region $IP = 7.5-11.3$ eV corresponding to π conjugated MOs, the OVGF calculations giving accurate band positions, and a combination of OVGF with EED should be used.

For the six highest bands in the cases of $\varphi = 0$, 45, and 90°, Figure 5 presents the electron density maps for MOs, the OVGF IPs, and the calculated EED spectra. The most noticeable feature

is a large shift (−0.92 eV from $\varphi = 0$ to 90°) for the position of band 5; at $\varphi = 90°$, it coincides with shifted band 6 (0.34 eV). Such a big shift is a good explanation for the absence of band 5 in the UPS and PIES spectra as well as for a structure between IP = 9.8 and IP = 10.6 eV. The broadening of band 1 and strong enhancing of the peak at IP = 9.3 eV can be explained in a similar way.

To obtain a calculated spectrum that can be compared with PIES, several spectra (Figure 5a) were synthesized by using the EED and OVGF values for $\varphi = 0-90°$. The total EED spectrum summed over a number of EED spectra from $\varphi = 0$ to 90° is presented in Figure 5a by the thick solid line below the measured PIES spectrum (dashed line). Both calculated and experimental spectra are in a good agreement with each other within the shift (−0.27 eV) between the scale of IP for the EED spectra and that of the electron energy for the PIES spectrum. The main part of this shift (−0.11 to −0.16 eV) is caused by the attractive interaction with the metastable He* atom at ionization from MOs related to the attractive regions of the target;[57] this difference is listed in the column (ΔE) in Table 1. Another reason for the shift of the EED spectra based on OVGF may be referred to the basis set error. Moreover, the following differences between the PIES and EED spectra can be noticed:

(i) In the case of phenylacetylene the typical divergence of the OVGF peak position for the highest π MO is ∼0.1 eV. A similar additional energy shift can be observed for the peak at $E_e = 8.85$ eV and for the left slope of the band at $E_e = 11.55$ eV.

(ii) The bands at $E_e = 11.55$ and 10.8 eV show some broadening in PIES, which can be connected to the vibrational structure of the C≡C bond stretching (Introduction, refs 37 and 38); the observed broadening of about 0.2 eV is in a good agreement with the stretching excitations (1557−2099 cm^{-1}).

Figure 4 presents the CERPIES of diphenylacetylene. Region of the "raised zero level" between $E_e = 9$ and $E_e = 10$ eV assigned to the shift of π' band 5 shows negative collision energy dependence of the cross-section with slope parameter $m = -0.23$ (Table 1).

Another region that cannot be assigned to any valence band but where a similar dependence of the ionization cross-section can be observed localizes at ca. $E_e = 6.65$ eV and is marked by S_1. Although the positions of bands 11 and 12 also shift at rotation (Table 2), the lowest energy for them (7.07 eV for band 12 1a, planar diphenylacetylene) is far from the observed structure. The most probable reason for that is the excitation of $\pi\pi^*(^1B_{1u})$ state with ionization,[36] which has already been observed by the 2D-PIES technique for benzene.[28] The S_1 can be related to the excitation at ionization from some bands in the peak at $E_e = 10.55$ eV; similar CEDPICS (Figure 6) slopes of the S_1 region and of bands 2, 3, and 4 ($m = -0.21$) are an argument for that, while an argument against is the difference of excitation energies in our case (∼3.9 eV) and in ref 36 (4.38 eV). It should also be noticed that region S_2 at $E_e = 3.7$ eV shows also the negative slope of CEDPICS ($m = -0.10$); a distance of ∼3.9 eV to the π bands 11 and 12 allow us to assume that a similar excitation process takes place. For phenylacetylene, similar structures S_1 and S_2 can also be noticed by CERPIES (Figure 2) at the same place. Since those structures are not observed clearly, we may only suppose that S_1 and S_2 in the case of phenylacetylene and diphenylacetylene have a common origin.

The CEDPICS data (Figure 6b) show that, as in the case of phenylacetylene, the most active part is the acetylene group, the MOs which localize mostly in the C≡C region and correspond to bands 5 and 6 have the largest absolute values of the slopes, $m = -0.23$ and −0.22, respectively. Other MOs with π character (except for band 1) have similar values of the CEDPICS slopes about $m = -0.21$. A smaller value ($m = -0.19$) for bands 11−12 can be explained by the influence of repulsive σ MOs 9 and 10 having IPs localized closely, and for $\varphi < 45°$ even between bands 11 and 12.

Because of structural similarities between both compounds investigated, we can expect that the interaction of planar diphenylacetylene with Li(2^2S) should have a character similar to that of phenylacetylene. The results of the Li model potential calculations (Figure 7b) confirm that assumption. Approach to the C≡C bond is repulsive for the in-plane direction and attractive for the out-of-plane one with a well depth of −84 meV. If dihedral angle φ increases until 45°, the directions corresponding to the ones mentioned above keep their attractive character of interaction. At $\varphi = 90°$, a natural equalization of these directions occurs; both of them become attractive with a relatively shallow well depth of −25 meV.

VI. Conclusion

The anisotropy of interaction potentials around phenylacetylene and diphenylacetylene molecules have been investigated by the collision-energy/ electron-energy-resolved 2D-PIES as well as the model calculations of interaction potential between the target molecule and He(2^3S) metastable atoms.

Two different functional groups, the acetylene and phenyl ones, form the molecules under investigation. These groups interact strongly with each other by the conjugation of π MOs. As a consequence, the spatial behavior of interaction with He-(2^3S) is different from that of benzene and acetylene.

According to the Li model potential calculations, attacks on the acetylene group in the plane of the phenyl and perpendicular to the phenyl group are not equivalent, even though both of them are perpendicular to the C≡C bond. In diphenylacetylene with a dihedral angle of 90°, these two directions of attack are equivalent, but the attractive behavior is strongly weakened by the closest hydrogen atoms of the phenyl groups; the well depth reaches −25 meV only. The anisotropy of interaction potential found by ab initio calculations should be understood in connection with the fact that all π MOs localized on the C≡C bond have similar characters of attractive interactions with He*-(2^3S) found by the observation of CEDPICS.

The interaction with the phenyl group is also different from that with benzene; so the well depth for phenylacetylene reaches a value of −57 meV, which seems not so deep as in the case of benzene (−107 meV).

Moreover, CERPIES and CEDPICS allow us to observe ionization accompanied by excitation that can be assigned to $\pi-\pi^*$ excitation at ionization from the π MOs localized mainly on the phenyl group; this kind of excitation is typical of benzenes.

Because of a low barrier of the torsional rotation about the C≡C bond, a diphenylacetylene molecule can be observed at room temperature not only in the most stable planar configuration but also in oscillation or rotation, with dihedral angles $\varphi = 0-90°$ between the planes of the phenyl groups. As a result, several types of π conjugation become possible, which causes several shapes of MOs to appear. Different ionization energies of such MOs were obtained by OVGF. So the position of a π band of the acetylene group shifts by 0.92 eV during rotation; this band can be observed in the spectra as a "raised zero level". Taking into consideration the change of the band position, an EED spectrum, which is in a good agreement with the measured PIES spectrum, was synthesized.

Acknowledgment. This work was supported by a Grant-in-Aid for Scientific Research from the Japanese Ministry of Education, Culture, Sports, Science, and Technology. A. B. is supported by the Research Fellowship of the Japan Society for the Promotion of Science for a JSPS postdoctoral fellowship (ID: P04384). M. Y. is supported by the Research Fellowship of the Japan Society for the Promotion of Science for Young Scientists.

References and Notes

(1) Penning, F. M. *Naturwissenschaften* **1927**, *15*, 818.
(2) Niehaus, A. *Adv. Chem. Phys.* **1981**, *45*, 399.
(3) Yencha, A. J. *Electron Spectroscopy: Theory, Technique and Applications*; Brundle, C. R., Berker, A. D., Eds.; Academic: New York, 1984; Vol. 5.
(4) Riola, J. P.; Haward, J. S.; Rundel, R. D.; Stebbings, R. F. *J. Phys. B* **1974**, *7*, 376.
(5) Lindinger, W.; Schmeltekopf, A. L.; Fehsenfelt, F. C. *J. Chem. Phys*. **1974**, *61*, 2890.
(6) Illenberger, E.; Niehaus, A. *Z. Phys. B* **1975**, *20*, 33.
(7) Pesnelle, A.; Watel, G.; Manus, C. *J. Chem. Phys*. **1975**, *62*, 3590.
(8) Woodard, M. R.; Sharp, R. C.; Seely, M.; Muschlitz, E. E., Jr. *J. Chem. Phys.* **1978**, *69*, 2978.
(9) Allison, W.; Muschlitz, E. E., Jr. *J. Electron Spectrosc. Relat. Phenom*. **1981**, *23*, 339.
(10) Parr, T. P.; Parr, D. M.; Martin, R. M. *J. Chem. Phys*. **1982**, *76*, 316.
(11) Appolloni, L.; Brunetti, B.; Hermanussen, J.; Vecchiocattivi, F.; Volpi, G. G. *J. Chem. Phys*. **1987**, *87*, 3804.
(12) Čermák, V. *J. Chem. Phys.* **1966**, *44*, 3781.
(13) Hotop, H.; Niehaus, A. *Z. Phys*. **1969**, *228*, 68.
(14) Ohno, K.; Mutoh, H.; Harada, Y. *J. Am. Chem. Soc.* **1983**, *105*, 4555.
(15) Ohno, K.; Matsumoto, S.; Harada, Y. *J. Chem. Phys.* **1984**, *81*, 4447.
(16) Mitsuke, K.; Takami, T.; Ohno, K. *J. Chem. Phys*. **1989**, *91*, 1618.
(17) Ohno, K.; Takami, T.; Mitsike, K.; Ishida, T. *J. Chem. Phys*. **1991**, *94*, 2675.
(18) Takami, T.; Mitsike, K.; Ohno, K. *J. Chem. Phys.* **1991**, *95*, 918.
(19) Takami, T.; Ohno, K. *J. Chem. Phys.* **1992**, *96*, 6523.
(20) Ohno, K.; Yamakado, H.; Ogawa, T.; Yamata, T. *J. Chem. Phys.* **1996**, *105*, 7536.
(21) Dunlavy, D. C.; Martin, D. W.; Siska, P. E. *J. Chem. Phys*. **1990**, *93*, 5347.
(22) Longley, E. J.; Dunlavy, D. C.; Falcetta, M. F.; Bevsek, H. M.; Siska, P. E. *J. Phys. Chem.* **1993**, *97*, 2097.
(23) Siska, P. E. *Rev. Mod. Phys.* **1993**, *65*, 337.
(24) Rothe, E. W.; Neynaber, R. H.; Trujillo, S. M. *J. Chem. Phys*. **1965**, *42*, 3310.
(25) Hotop, H. *Radiation Res.* **1974**, *59*, 379.
(26) Haberland, H.; Lee, Y. T.; Siska, P. E. *Adv. Chem. Phys.* **1981**, *45*, 487.
(27) Yamazaki, M.; Maeda, S.; Kishimoto, N.; Ohno, K. *J. Chem. Phys.* **2002**, *117*, 5707.
(28) Yamazaki, M.; Maeda, S.; Kishimoto, N.; Ohno, K. *J. Chem. Phys*. **2005**, *122*, 044303.
(29) Ohno, K. *Bull. Chem. Soc. Jpn.* **2004**, *77*, 887.
(30) Ohno, K.; Okamura, K.; Yamakado, H.; Hoshino, S.; Takami, T.; Yamauchi, M. *J. Phys. Chem.* **1995**, *99*, 14247.
(31) Pasinszki, T.; Kishimoto, N.; Ohno, K. *J. Phys. Chem. A* **1999**, *103*, 9195.
(32) Kishimoto, N.; Osada, Y.; Ohno, K. *J. Phys. Chem. A* **2000**, *104*, 1393.
(33) Kishimoto, N.; Yamakado, H.; Ohno, K. *J. Phys. Chem.* **1996**, *100*, 8204.
(34) Yamakado, H.; Yamauchi, M.; Hoshino, S.; Ohno, K. *J. Phys. Chem.* **1995**, *99*, 17093.
(35) Okuyama, K.; Hasegawa, T.; Ito, M.; Mikami, N. *J. Phys. Chem.* **1984**, *88*, 1711.
(36) Okuyama, K.; Cockett, M. C. R.; Kimura, K. *J. Chem. Phys*. **1992**, *97*, 1649.
(37) Kellerer, B.; Hacker H. H. *J. Mol. Struct*. **1972**, *13*, 79.
(38) Hiura, H.; Takahashi, H. *J. Phys. Chem.* **1992**, *96*, 8909.
(39) Ishibashi, T.; Hamaguchi, H. *Chem. Phys. Lett*. **1997**, *264*, 551
(40) Mayer, J. P.; Turner, D. W. *Faraday Soc*. **1972**, *54*, 149.
(41) Griebel, P.; Hohlneicher, G.; Dörr, F. *J. Electron Spec. Relat. Phenom*. **1974**, *4*, 185.
(42) Elbel, S.; Lienert, K.; Krebs, A.; tom Deick., H. *Liebigs Ann. Chem.* **1981**, 1785.
(43) Horio, T.; Hatamoto, T.; Kishimoto, N.; Ohno,K. *Chem. Phys. Lett.* **2004**, *397*, 242.
(44) Ohno, K.; Yamazaki, M.; Maeda, S.; Kishimoto, N. *J. Electron Spectrosc. Relat. Phenom*. **2005**, *142*, 283.
(45) Maeda, S.; Yamazaki, M.; Kishimoto, N.; Ohno, K. *J. Chem. Phys.* **2004**, *120*, 781.
(46) Kishimoto, N.; Hagihara, Y.; Ohno, K.; Knippenberg, S.; Francois, J.-P.; Deleuze, M. S. *J. Phys. Chem. A* **2005**, *109*, 10535.
(47) Kishimoto, N.; Aizawa, J.; Yamakado, H.; Ohno, K. *J. Phys. Chem. A* **1997**, *101*, 5038.
(48) Gardner, J. L.; Samson, J. A. R. *J. Electron Spectrosc. Relat. Phenom*. **1976**, *8*, 469.
(49) Kimura, K.; Katsumata, S.; Achiba, Y.; Yamazaki, T.; Iwata, S. *Handbook of HeI Photoelectron Spectra of Fundamental Organic Molecules*; Japan Scientific: Tokyo, 1981.
(50) Cederbaum, L. S.; Domcke, W. *Adv. Chem. Phys.* **1977**, *36*, 205.
(51) von Niessen, W.; Schirmer, J.; Cederbaum, L. S. *Comput. Phys. Rep*. **1984**, *1*, 57.
(52) Ortiz, J. V. *J. Chem. Phys*. **1988**, *89*, 6348.
(53) Cox, A. P.; Ewart, I. C.; Stigliani, W. M. *J. Chem. Soc., Faraday Trans*. **1975**, *71*, 504.
(54) Abramenkov, A. V.; Almeningen, A. *Acta Chem. Scand.; Ser. A.* **1988**, *42*, 674.
(55) Boys, S. F.; Bernardi, F. *Mol. Phys.* **1970**, *10*, 553.
(56) Frisch, A. et al. *Gaussian 03*; Gaussian, Inc., Wallingford CT, 2004.
(57) Niehaus, A. *Ber. Bunsen-Ges. Phys. Chem.* **1973**, *77*, 632.